# Simulating the birth environment of circumstellar discs

Concha Ramirez, F.A.

Cover Page

# 3 | External photoevaporation of circumstellar discs constrains the time-scale for planet formation

**F. Concha-Ramírez**; M. J. C. Wilhelm;
S. Portegies Zwart; T. J. Haworth

Planet-forming circumstellar discs are a fundamental part of the star formation process. Since stars form in a hierarchical fashion in groups of up to hundreds or thousands, the UV radiation environment that these discs are exposed to can vary in strength by at least six orders of magnitude. This radiation can limit the masses and sizes of the discs. Diversity in star forming environments can have long lasting effects in disc evolution and in the resulting planetary populations. We perform simulations to explore the evolution of circumstellar discs in young star clusters. We include viscous evolution, as well as the impact of dynamical encounters and external photoevaporation. We find that photoevaporation is an important process in destroying circumstellar discs: in regions of stellar density $\rho \sim 100 \, \mathrm{M}_\odot \, \mathrm{pc}^{-3}$ around 80% of discs are destroyed before 2.0 Myr of cluster evolution. In regions of $\rho \sim 50 \, \mathrm{M}_\odot \, \mathrm{pc}^{-3}$ around 50% of discs are destroyed in the same timescale. Our findings are in agreement with observed disc fractions in young star forming regions and support previous estimations that planet formation must start in timescales $< 0.1 - 1$ Myr.

✳

## 3.1.    Introduction

Circumstellar discs develop as a result of the star formation process (Williams & Cieza 2011). Since a non negligible fraction of stars are not born in isolation (Bressert et al. 2010; King et al. 2012), and gas left over from the star formation process can linger for a few Myr (Portegies Zwart et al. 2010), during their first stages of evolution the discs remain embedded in an environment that is dense in gas and neighbouring stars. These conditions can be hostile for the discs in a myriad of ways: they can be subject to dynamical truncations (Vincke et al. 2015; Portegies Zwart 2016; Vincke & Pfalzner 2016) or be affected by processes related to stellar evolution, such as stellar winds (Pelupessy & Portegies Zwart 2012), supernovae explosions (Close & Pittard 2017; Portegies Zwart et al. 2018), and photoevaporation due to bright OB stars in the vicinity (e.g. Guarcello et al. 2016; Haworth et al. 2017). The surrounding gas can also shrink the discs through ram pressure stripping (Wijnen et al. 2016, 2017a). Since planet formation related processes seem to start very quickly in circumstellar discs ($< 0.1 - 1\,\mathrm{Myr}$, Najita & Kenyon (2014); Manara et al. (2018)), understanding the mechanisms that affect disc evolution is directly connected to understanding planetary system formation and survival. The Sun was probably born within a star cluster (Portegies Zwart et al. 2009), so discerning how the cluster environment affects the evolution of the discs can help us comprehend the origins of the Solar System.

There are several observational indications that the environment of circumstellar discs shortly after their formation is unfavourable for their survival. Discs have been observed to be evaporating in several young star forming regions (e.g. Fang et al. 2012; de Juan Ovelar et al. 2012; Mann et al. 2014; Kim et al. 2016; van Terwisga et al. 2019). Moreover, observations indicate that disc fractions decline in regions close to an O-type star (e.g. Balog et al. 2007; Guarcello et al. 2007, 2009, 2010; Fang et al. 2012; Mann et al. 2014; Guarcello et al. 2016). Fatuzzo & Adams (2008) estimate an FUV radiation field of up to $G_0 \approx 1000$ in star clusters of $N > 1000$ stars[1], while Facchini et al. (2016) show that discs of radius $\sim 150\,\mathrm{au}$ are subject to photoevaporation even in very low FUV fields ($G_0 = 30$). In regions of high stellar density, nearby stars can also affect disc size and morphology by dynamical interactions. Observational evidence of the imprints of dynamical truncations has been reported in several nearby stellar clusters (Olczak et al. 2008; Reche et al. 2009; de Juan Ovelar et al. 2012). Tidal stripping that can be explained by disc-star interactions has been observed in the RW Aurigae system (Cabrit et al. 2006; Rodriguez et al. 2018; Dai et al. 2015) and in the T Tauri binary system AS 205 (Salyk et al. 2014). There is also evidence that the Solar System might have been affected by a close encounter with another star during its early stages (Jílková et al. 2015; Pfalzner et al. 2018).

Circumstellar discs are not only affected by external processes, but also by their internal viscous evolution. The combination of outwardly decreasing angular velocity together with outwardly increasing angular momentum causes shear stress forces inside the discs. As a consequence mass is accreted from the innermost regions of the disc onto its host star, whereas the outermost regions expand (Lynden-Bell & Pringle 1974). Tazzari et al. (2017) propose that the measured offsets in sizes and masses of discs in the Lupus clouds versus discs in the Taurus-Auriga and Ophiuchus regions can be explained as observational evidence of viscous spreading. However Rosotti et al. (2019) argue that current surveys do not yet have the sufficient sensitivity to properly detect this phenomenon.

Different approaches have been implemented to study the effects of these processes on the lifetime of circumstellar discs. External photoevaporation has been modelled with radiation hydrodynamics codes that solve flow equations through the disc boundaries, together

---

[1]$G_0$ is the FUV field measured in units of the Habing flux, $1.6 \times 10^{-3}\,\mathrm{erg\,s^{-1}\,cm^{-2}}$ (Habing 1968).

with photodissociation region codes to obtain the temperature profiles of the discs (e.g. Haworth et al. 2016; Facchini et al. 2016). This method has been coupled with $\alpha$-disc models to account for viscous evolution of the disc (e.g. Adams et al. 2004; Anderson et al. 2013; Gorti et al. 2015; Rosotti et al. 2017). Haworth et al. (2018a) introduce the concept of pre-computing photevaporation mass losses in terms of the surface density of the discs, an approach that we expand on in section 3.2.3. Winter et al. (2019a) model the environment of Cygnus OB2 and use the photoevaporation mass loss rate to constrain the timescale for gas expulsion in the young star forming region. Nicholson et al. (2019) perform simulations of star forming regions where FUV photoevaporation is implemented in post-processing, and find a very short lifetime for the discs ($< 2\,\mathrm{Myr}$) in moderate and low density regions ($\lesssim 100\,\mathrm{M_\odot\,pc^{-3}}$).

Regarding dynamical effects, close encounters on a single N-body disc of test particles have been investigated in several studies (e.g. Breslau et al. 2014; Jílková et al. 2016; Bhandare et al. 2016; Pfalzner et al. 2018). Winter et al. (2018a,b) use a ring of test particles around a star to obtain linearized expressions of the effect that a stellar encounter can have on the mass and morphology of the disc, and then use them to simulate the disc using a smoothed particles hydrodynamics (SPH) code. A different approach for studying these effects is evolving the stellar dynamics of the cluster separately, and applying the effects of dynamical encounters afterwards (e.g. Olczak et al. 2006, 2010; Malmberg et al. 2011; Steinhausen & Pfalzner 2014; Vincke et al. 2015; Vincke & Pfalzner 2016, 2018). Directly adding SPH discs to a simulation of a massive star cluster is computationally expensive, since a high resolution is needed over long time scales. The closest effort corresponds to the work by Rosotti et al. (2014), in which individual SPH codes are coupled to half of the $1\,\mathrm{M_\odot}$ stars in a cluster with 100 stars. This allows them to study the effects of viscous spreading of the discs and dynamical truncations in a self-consistent way, but they are limited by the computational resources needed for this problem. Parametrized approaches have also been developed, where the cluster dynamics and effects of truncations (Portegies Zwart 2016) and viscous spreading (Concha-Ramírez et al. 2019a) are considered simultaneously.

Concha-Ramírez et al. (2019a) investigate the effect of viscous growth and dynamical truncations on the final sizes and masses of protoplanetary discs inside stars clusters using a parametrized model for the discs. They show that viscous evolution and dynamical encounters are unable to explain the compact discs observed in star forming regions. They argue that other processes must affect the early evolution of the discs. Here we expand the model by improving the description of the viscous discs and by adding external photoevaporation due to the presence of bright nearby stars.

We model the circumstellar discs using the Viscous Accretion Disc Evolution Resource (VADER) (Krumholz & Forbes 2015). This code solves the equations of angular momentum and mass transport in a thin, axisymmetric disc. Dynamical truncations are parametrized, and the mass loss due to external photoevaporation is calculated using the Far-ultraviolet Radiation Induced Evaporation of Discs (FRIED) grid (Haworth et al. 2018b). This grid consists of pre-calculated mass loss rates for discs of different sizes and masses, immersed in several different external FUV fields. We use the Astrophysical Multipurpose Software Environment (AMUSE[2], Portegies Zwart & McMillan 2018) framework to couple these codes along with cluster dynamics and stellar evolution. All the code developed for the simulations, data analyses, and figures of this paper is available in Github[3].

---

[2]http://amusecode.github.io/
[3]https://doi.org/10.5281/zenodo.3537675

## 3.2. Model

### 3.2.1. Viscous growth of circumstellar discs

We implement circumstellar discs using the Viscous Accretion Disc Evolution Resource (VADER) by Krumholz & Forbes (2015). VADER is an open source viscous evolution code which uses finite-volume discretization to solve the equations of mass transport, angular momentum, and internal energy in a thin, axisymmetric disc. An AMUSE interface for VADER was developed in the context of this work and is available online.

For the initial disc column density we use the standard disc profile introduced by Lynden-Bell & Pringle (1974):

$$\Sigma(r, t = 0) = \Sigma_0 \frac{r_c}{r} \exp\left(\frac{-r}{r_c}\right), \tag{3.1}$$

with

$$\Sigma_0 = \frac{m_d}{2\pi r_c^2 \left(1 - \exp\left(-r_d/r_c\right)\right)}, \tag{3.2}$$

where $r_c$ is the characteristic radius of the disc, $r_d$ and $m_d$ are the initial radius and mass of the disc, respectively, and $\Sigma_0$ is a normalization constant. Considering $r_c \approx r_d$ (Anderson et al. 2013), the density profile of the disc is:

$$\Sigma(r, t = 0) \approx \frac{m_d}{2\pi r_d \left(1 - e^{-1}\right)} \frac{\exp(-r/r_d)}{r}. \tag{3.3}$$

This expression allows the disc to expand freely at the outer boundary while keeping the condition of zero torque at the inner boundary $r_i$.

To establish the radius of the discs we set the column density outside $r_d$ to a negligible value $\Sigma_{edge} = 10^{-12}$ g cm$^{-2}$. The FRIED grid that we use to calculate the photoevaporation mass loss (see section 3.2.3) is a function of disc radius and outer surface density. There is a numerical challenge in determining what the disc outer surface density and radius actually are, since there is a large gradient in it down to the $\Sigma_{edge}$ value. Computing a mass loss rate for a very low outer surface density in this steep gradient would return an artificially low result. Considering this we define the disc radius as the position of the first cell next to $\Sigma_{edge}$, as shown in Figure 3.1.

The temperature profile of the discs is given by

$$T(r) = T_m \left(\frac{r}{1 \text{ au}}\right)^{-1/2}, \tag{3.4}$$

where $T_m$ is the midplane temperature at 1 au. Based on Anderson et al. (2013) we adopt $T_m = 300$ K.

Each disc is composed of a grid of 50 logarithmically spaced cells, in a range between 0.5 and 5000 au. In Appendix 3.A we show that the resolution is enough for our calculations. The discs have a Keplerian rotation profile and turbulence parameter $\alpha = 5 \times 10^{-3}$. The fact that the outer radius of the grid is much larger than the disc sizes (which were initially around 100 au, see section 3.2.4) allows the discs to expand freely without reaching the boundaries of the grid. The mass flow through the outer boundary is set to zero in order to maintain the density $\Sigma_{edge}$ needed to define the disc radius. The mass flow through the inner boundary is considered as accreted mass and added to the mass of the host star.
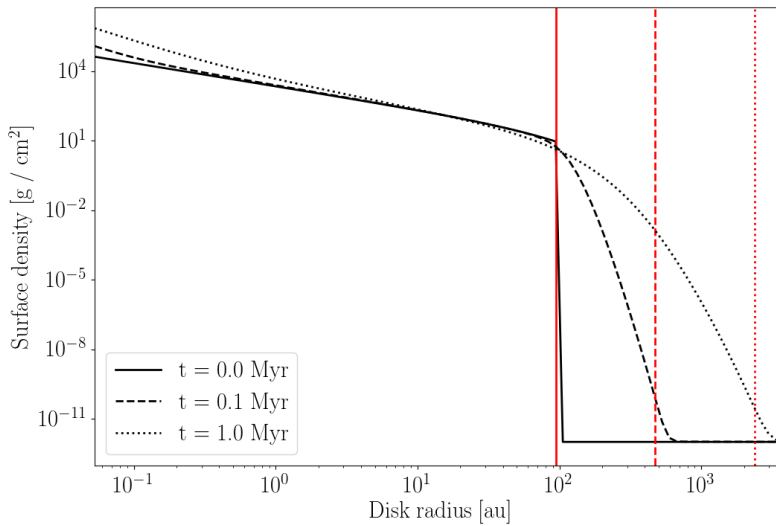
Figure 3.1: Definition of disc radius. The black lines show the disc profile and the corresponding red lines show the measured disc radius. Solid lines represent a disc initialized with $R = 100$ au. The dashed lines show the same disc after 0.1 Myr of isolated evolution, and the dotted lines after 1.0 Myr of isolated evolution.

### 3.2.2. Dynamical truncations

A close encounter between discs induces a discontinuity in their evolution. To modify the discs we calculate parametrized truncation radii. For two stars of the same mass, Rosotti et al. (2014) approximated the truncation radius to a third of the encounter distance. Together with the mass dependence from Bhandare et al. (2016), the dynamical truncation radius takes the form:

$$r' = \frac{r_{enc}}{3} \left( \frac{m_1}{m_2} \right)^{0.32}, \tag{3.5}$$

where $m_1$ and $m_2$ are the masses of the encountering stars.

To implement truncations we first calculate the corresponding truncation radius caused by the encounter, according to equation 3.5. We consider all the mass outside this radius to be stripped from the disc. To define $r'$ as the new disc radius we change the column density of all the disc cells outside $r'$ to the edge value $\Sigma_{edge} = 10^{-12}$ g cm$^{-2}$.

### 3.2.3. External photoevaporation

A circumstellar disc can be evaporated by radiation coming from its host star or from a bright star in the vicinity. The heating of the disc surface can lead to the formation of gaps at different locations, which can cause the progression to a transition disc (e.g. Clarke et al. 2001; Gorti et al. 2009). The radiation can also truncate the disc by removing material from the outer, loosely-bound regions (e.g. Adams et al. 2004).

Models of internal photoevaporation have shown that most of the mass loss in this case occurs in the inner 20 au of the disc (Font et al. 2004; Owen et al. 2010). Radiation from the

host star can evaporate material from the outskirts of the disc, however Owen et al. (2010) show that more than 50% of the total mass loss occurs in the $5 - 20$ au region. In Font et al. (2004) around 90% of the mass loss occurs within the inner 18 au of the disc. Given that the mass loss rate from the outer disc is typically comparable to or larger than that from the inner disc, we expect external photoevaporation to dominate in the outer regions. External photoevaporation has been shown to be more effective in evaporating the discs than radiation from the host star (e.g. Johnstone et al. 1998; Adams & Myers 2001). Truncation by external photoevaporation can also result in changes of the viscosity parameter $\alpha$, which further affects the viscous evolution of the discs (Rosotti et al. 2017). In this work we ignore the effects of photoevaporation on internal disc structure, and deal exclusively with disc survival rates. Because of this and the discussion above we focus on external photoevaporation due to bright stars in the vicinity.

OB-type stars emit heating radiation in the form of extreme-ultraviolet (EUV), far-ultraviolet (FUV), and X-rays. In the case of external photoevaporation the dispersal of disc material is dominated by the FUV photons (Armitage 2000; Adams et al. 2004; Gorti & Hollenbach 2009). The main part of our work deals with photoevaporation due to FUV photons; in addition we also incorporate the effect of EUV photons (see Eq. 5.4).

The amount of mass lost from the discs as a result of external photoevaporation depends on the luminosity of the bright stars in the cluster. This luminosity, together with the distance from each of the massive stars to the discs, is used to obtain the amount of radiation received by each disc. We can then calculate the amount of mass lost. Below we explain what we consider to be massive stars and how we calculate the mass loss rate.

**FUV luminosities**

We follow Adams et al. (2004) in defining the FUV band ranging from 6 eV up to 13.6 eV, or approximately from 912 ÃĚ to 2070 ÃĚ. We calculate the FUV radiation of the stars in the simulations based on their spectral types. Given the presence of spectral lines in this band, we use synthetic stellar spectra rather than relying on black body approximations. The spectral library used is UVBLUE (Rodriguez-Merino et al. 2005), chosen for its high coverage of parameter space and high resolution, spanning the appropriate wavelength ranges. It spans a three dimensional parameter space of stellar temperature, metallicity, and surface gravity.

We use the UVBLUE spectral library to precompute a relation between stellar mass and FUV luminosity. We do this by considering all the stars in the cluster to have solar metallicity (Z = 0.02). We then select the temperature and surface gravity spectra closer to the zero age main sequence value of each star, according to the parametrized stellar evolution code SeBa (Portegies Zwart & Verbunt 1996; Toonen et al. 2012). Given that the masses and radii of the stars are known, using the chosen spectra we build a relationship between stellar mass and FUV luminosity. This relation takes the shape of a segmented power law, as is shown in Figure 3.2. A similar fit was obtained by Parravano et al. (2003). In runtime the stars are subject to stellar evolution and the FUV luminosity for each star was calculated directly from this fit using the stellar mass.

The mass range of the fit in Figure 3.2 is $0.12 - 100$ M$_\odot$, however, we are only interested in the range $1.9 - 50$ M$_\odot$. As is further explained in section 3.2.3, we only consider stars with masses higher that 1.9 M$_\odot$ to be emitting FUV radiation, and 50 M$_\odot$ is the theoretical upper limit for the stellar mass distribution. Stars with masses $\leq$ 1.9 M$_\odot$ are given discs and are affected by the massive stars. The massive stars are also subject to stellar evolution, which is implemented with SeBa through the AMUSE interface. The FUV luminosity of each massive star is calculated in every time step, from the precomputed fit, after evolving the stellar
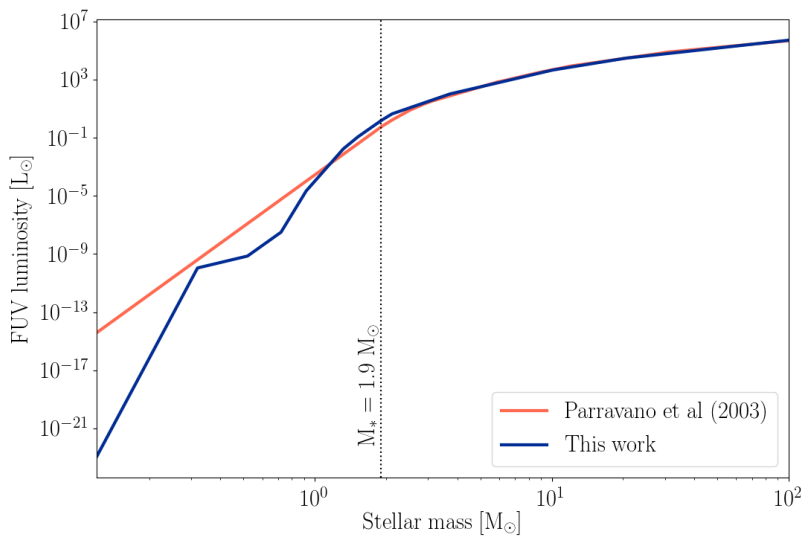
Figure 3.2: FUV luminosity vs. stellar mass fit calculated from the ZAMS spectra. $M_* = 1.9\,M_\odot$ is the lower mass limit of the FRIED grid, and the lower mass limit for the stars to be considered emitting FUV radiation in our simulations (see Section 3.2.3 for details).

evolution code. The low mass stars are not subject to stellar evolution.

### Mass loss rate due to external photoevaporation

To calculate the mass loss due to FUV external photoevaporation we use the Far-ultraviolet Radiation Induced Evaporation of Discs (FRIED) grid developed by Haworth et al. (2018b). The FRIED grid is an open access grid of calculations of externally evaporating circumstellar discs. It spans a five dimension parameter space consisting of disc sizes ($1 - 400$ au), disc masses ($10^{-4} - 10^2\,M_{Jup}$), FUV fields ($10 - 10^4\,G_0$), stellar masses ($0.05 - 1.9\,M_\odot$) and disc outer surface densities. The seemingly three dimensional grid subspace of disc mass, edge surface density, and disc radius is in fact two dimensional, as any combination of disc radius and disc mass has only one edge density associated with it. Because of this, we only take into account a four dimensional grid of radiation field strength, host star mass, disc mass, and disc radius.

Following the stellar mass ranges of the FRIED grid we separate the stars in the simulations into two subgroups: *massive stars* and *low mass stars*. Massive stars are all stars with initial masses higher than $1.9\,M_\odot$, while low mass stars have masses $\leq 1.9\,M_\odot$. Only the low mass stars have circumstellar discs in the simulations. The massive stars are considered as only generating FUV radiation and affecting the low mass stars. In this way we make sure that we stay within the stellar mass limits of the FRIED grid. Low mass stars ($\lesssim 1\,M_\odot$) have a negligible UV flux (Adams et al. 2006), so this approximation holds well for our purposes. Calculation of the FUV radiation emitted by the massive stars is further explained in section 3.2.3. These star subgroups are considered only for the calculation of FUV radiation and photoevaporation mass loss. In the gravity evolution code the two subgroups are undistinguishable.

The FRIED grid allows to take a circumstellar disc with a specific mass, size, and density,

around a star with a certain mass, and from the FUV radiation that it receives, obtain the photoevaporation mass loss. However, the parameters of the simulated discs do not always exactly match the ones in the grid. We perform interpolations over the grid to calculate the mass losses of the discs in the simulations. Because of computational constraints, we perform the interpolations on a subspace of the grid, such that it contains at least one data point above and below the phase space point of the disc in each dimension. The high resolution of the FRIED grid ensures that this interpolation is performed over an already smooth region.

When a massive star approaches a circumstellar disc, external photoevaporation is dominated by EUV radiation. Following Johnstone et al. (1998) we define a distance limit below which EUV photons dominate:

$$d_{min} \simeq 5 \times 10^{17} \left( \frac{\epsilon^2}{f_r \Phi_{49}} \right)^{-1/2} r_{d_{14}}^{1/2} \text{ cm} \tag{3.6}$$

where $\left( \frac{\epsilon^2}{f_r \Phi_{49}} \right)^{1/2} \approx 4$, $r_{d_{14}} = \frac{r_d}{10^{14} cm}$ with $r_d$ the disc radius, and $5 \times 10^{17}$ cm $\sim 3 \times 10^4$ au $\sim$ 0.16 pc. When a star with a disc is at a distance $d < d_{min}$ from a massive star we calculate the mass loss using equation (20) from Johnstone et al. (1998):

$$\dot{M}_{EUV} = 2.0 \times 10^{-9} \frac{(1+x)^2}{x} \epsilon r_{d_{14}} M_{\odot} \text{ yr}^{-1} \tag{3.7}$$

with $x \approx 1.5$ and $\epsilon \approx 3$. During most of their evolution, however, the circumstellar discs in the simulations experience photoevaporation only due to FUV photons. Since we do not consider interstellar gas and dust in the clusters, we do not account for extinction in the calculation of the radiation received by each small star.

**Disc truncation due to photoevaporation**

Once the mass loss due to photoevaporation is calculated for every disc, the discs are truncated at a point that coincides with the amount of mass lost in the process. We take the approach of Clarke (2007) and remove mass from the outer edge of the disc. We do this by moving outside-in from the disc edge and removing mass from each cell by turning its column density to the edge value $\Sigma_{\text{edge}} = 10^{-12}$ defined in section 3.2.1. We stop at the point where the mass removed from the disc is equal to the calculated mass loss.

We consider a disc to be completely evaporated when it has lost 99% of its initial mass (Anderson et al. 2013) or when its mean column density is lower than 1 g cm$^{-2}$ (Pascucci et al. 2016). From this point forward the star continues its dynamical evolution normally, but is no longer affected by massive stars.

**Summary of cluster evolution**

The code runs in major time steps, which represent the time scale on which the various processes are coupled. Within each of these macroscopic time steps (1000 yr), internal evolutionary processes such as stellar evolution and gravitational dynamics proceed in their own internal time steps (500 yr and 1000 yr respectively). Throughout each macroscopic time step, we perform the following operations:

1. Gravitational dynamics code is evolved.

2. We check the stars for dynamical encounters:

   2.a  If a dynamical encounter occurs, we determine the truncation radius for each disc.

    2.b  We update the radius and mass of the discs.

3.  Stellar evolution code is evolved.

4.  Photoevaporation process is carried out as follows. For each massive star:

    4.a  We calculate the distance $d$ from the massive star to each low mass star.

    4.b  If $d < d_{min}$ (see Eq. 5.4) we calculate the mass loss $\dot{M}_{EUV}$.

    4.c  If $d \geq d_{min}$ the massive star's FUV luminosity $L_{FUV}$ is calculated (see section 3.2.3).

    4.d  Using $d$ and $L_{FUV}$ we calculate $l_{FUV}$, the amount of FUV radiation received by the low mass star.

    4.e  Using $l_{FUV}$ together with the low mass star's mass, disc mass, and disc radius, we build a sub-grid of the FRIED grid and interpolate over it to calculate the mass loss $\dot{M}_{FUV}$.

    4.f  The total mass loss in the time step is calculated using $\dot{M}_{EUV}$ and $\dot{M}_{FUV}$.

    4.g  The mass is removed from the disc by moving outside-in and removing mass from the cells.

    4.h  The disc mass and radius are updated.

5.  Discs are checked for dispersal. If a disc has been dispersed (see section 3.2.3) the code for the disc is stopped and removed and the star continues evolving only as part of the gravitational dynamics code.

6.  Simulation runs until 5 Myr of evolution of until all the discs are dispersed, whichever happens first.

    We present a scheme of this process and of the photoevaporation in Figures 3.3 and 3.4 respectively.

### 3.2.4.   Initial conditions

**Discs**

    The initial radii of the circumstellar discs are given by:

$$R_d(t = 0) = R' \left( \frac{M_*}{M_\odot} \right)^{0.5} \tag{3.8}$$

where $R'$ is a constant. The youngest circumstellar discs observed to date have diameters that range from $\sim$ 30 au (e.g. Lee et al. 2018) to $\sim 120 - 180$ au (e.g. Murillo et al. 2013; van 't Hoff et al. 2018). Based on this we choose $R' = 100$ au, which for our mass range $0.05 - 1.9$ M$_\odot$ for stars with discs results in initial disc radii between $\sim$ 22 au and $\sim$ 137 au.

    The initial masses of the discs are defined as:
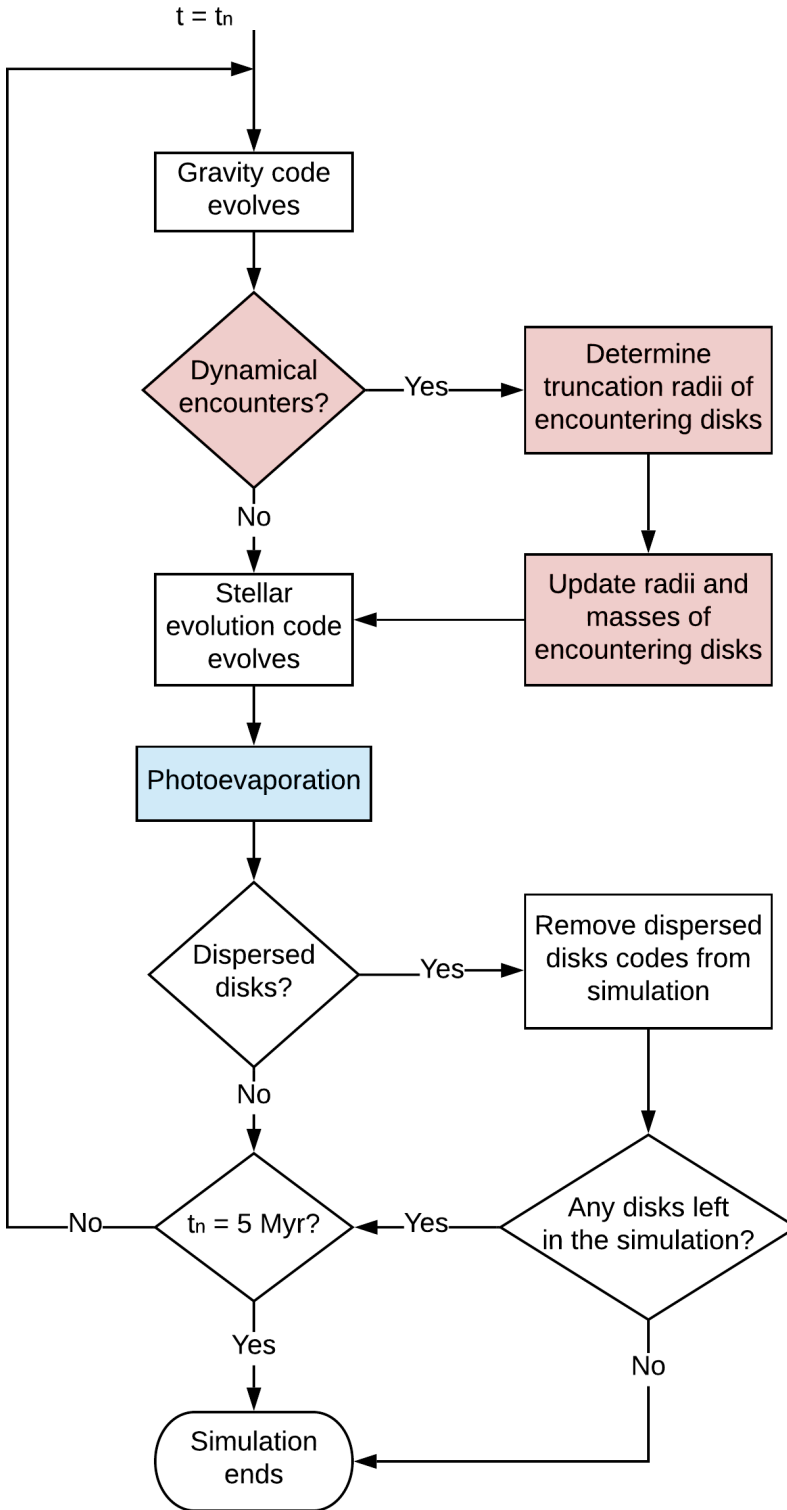
$$M_d(t = 0) = 0.1 M_* \tag{3.9}$$

Figure 3.3: Operations performed in each macroscopic time step. Within each macroscopic time step $t_n$, internal evolutionary processes such as stellar evolution and gravitational dynamics proceed in their own internal time steps.
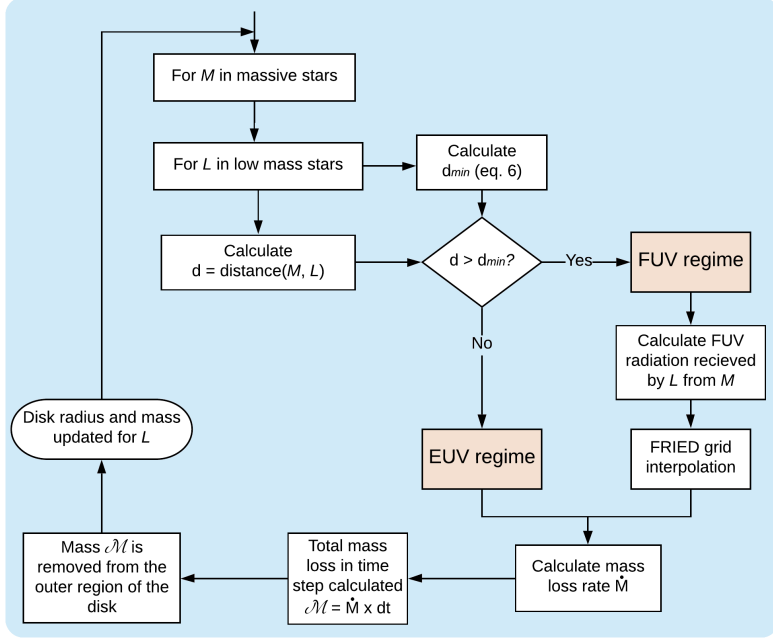
Figure 3.4: Flowchart of the photoevaporation process.

| Region | Sim. # | Low mass stars | $\overline{M}_{\text{low mass}}[\ M_\odot]$ | Massive stars | $\overline{M}_{\text{massive}}[\ M_\odot]$ |
|---|---|---|---|---|---|
| | 1 | 97% | $1.18 \pm 0.17$ | 3% | $4.08 \pm 2.69$ |
| $\rho_{100}$ | 2 | 99% | $0.24 \pm 0.30$ | 1% | 3.43 |
| | 3 | 96% | $0.24 \pm 0.31$ | 4% | $4.51 \pm 2.59$ |
| | 1 | 94% | $0.27 \pm 0.33$ | 6% | $5.94 \pm 5.65$ |
| $\rho_{50}$ | 2 | 96% | $0.25 \pm 0.31$ | 4% | $3.51 \pm 0.26$ |
| | 3 | 99% | $0.24 \pm 0.27$ | 1% | 4.90 |

Table 3.1: Stellar mass properties in each simulation run.

## Cluster

We perform simulations of young star clusters with stellar densities $\rho \sim 100\ M_\odot\ \text{pc}^{-3}$ and $\rho \sim 50\ M_\odot\ \text{pc}^{-3}$ using Plummer sphere spatial distributions (Plummer 1911). We will refer to these distributions as $\rho_{100}$ and $\rho_{50}$, respectively. All the regions are in virial equilibrium (viral ratio $Q = 0.5$).

Stellar masses are randomly drawn from a Kroupa mass distribution (Kroupa 2001) with maximum mass $50\ M_\odot$. The mean mass of the distribution is $\overline{M}_* \approx 0.3\ M_\odot$. In Table 3.1 we show the details of the stellar masses in each simulation.

The simulations end at 5 Myr or when all the discs are dispersed, whichever happens first.
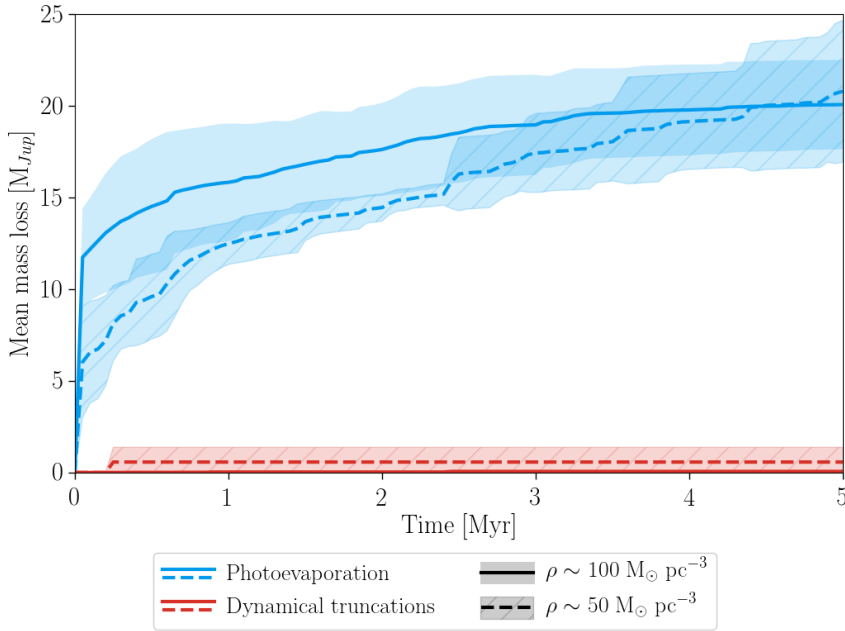
Figure 3.5: Mean mass loss in time due to external photoevaporation (blue) and dynamical truncations (red). The solid and dashed lines correspond to the $\rho_{100}$ and $\rho_{50}$ regions, respectively. The shaded areas indicate the standard deviation of the simulations.

## 3.3.   Results

### 3.3.1.   Disc mass loss in time

As a way to quantify the mass loss effect of each of the processes included in the simulations, we measure the mass loss due to external photoevaporation and dynamical truncations separately. In Figure 3.5 we show the mass loss over time for external photoevaporation and dynamical truncations. The solid and dashed lines correspond to the mean mass loss among all stars in the $\rho_{100}$ and $\rho_{50}$ regions, respectively. The shaded areas show the extent of the results in the different simulation runs.

The mass lost from the circumstellar discs is dominated by external photoevaporation over the entire lifetime of the simulated clusters. Dynamical truncations only have a local effect on truncating disc radii and masses, whereas photoevaporation is a global effect influencing all discs in the cluster.

The amount of FUV radiation received by each disc and the ensuing mass loss are variable. The effect depends on the proximity to massive stars, which changes with time as the stars orbit in the cluster potential. For the $\rho_{100}$ region the average FUV radiation over 5 Myr of evolution was $\sim 475$ $G_0$, with a minimum of 10 $G_0$ and a maximum of $\sim 10^4$ $G_0$. For the $\rho_{50}$ region the average over 5 Myr was $\sim 56$ $G_0$, minimum $\sim 2$ $G_0$ and maximum 267 $G_0$. These values are only shown as an indicative of the environment that the simulation discs were dispersed in, however a short exposure to a strong FUV field can be instantly more destructive than a sustained low FUV field. The FUV field can also vary in time due to processes intrinsic to star formation, such as a massive star being embedded during its early stages (e.g. Ali & Harries 2019). In our simulations, however, photoevaporation is driven by
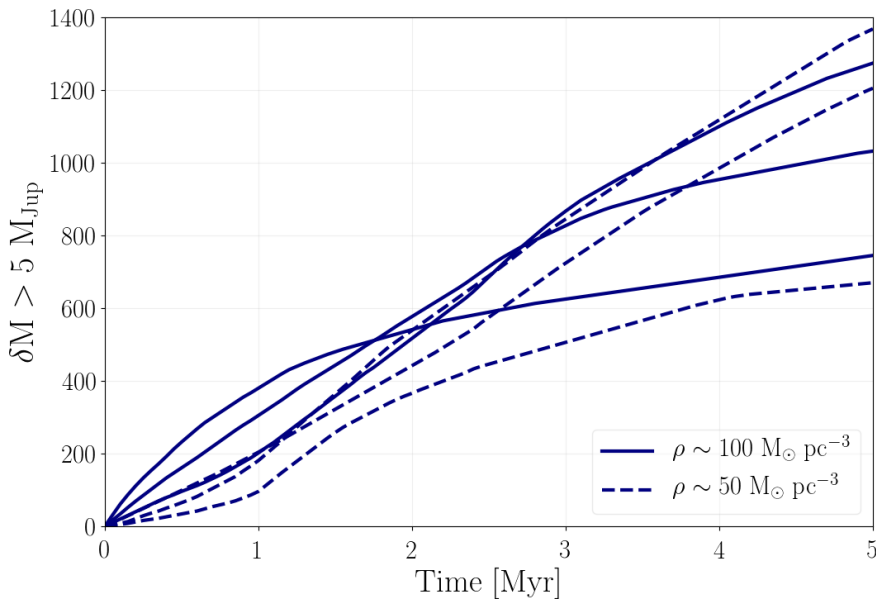
Figure 3.6: Cumulative distribution of discs that lose more than 5 $M_{Jup}$ in time in each simulation. The solid lines correspond to the $\rho_{100}$ region simulations and the dashed lines to the $\rho_{50}$ region simulations.

the background FUV field. In Figure 3.6 we show the cumulative distributions of discs that lose more than 5 $M_{Jup}$ in time. It can be seen that large mass losses are not driven by close encounters with bright stars but by the environmental FUV radiation. From Figure 3.6 it can be seen that before 2 Myr of evolution the discs in $\rho_{100}$ lose mass more strongly than the ones in $\rho_{50}$. However, starting around 2 Myr and until the end of the simulations there is large scatter in the mass loss behaviour for each region. This is related to the dynamics of each cluster. For $\rho_{100}$ the crossing time is $t_{cross} = 1.20 \pm 0.04$ Myr, and for $\rho_{50}$ the crossing time is $t_{cross} = 0.98 \pm 0.09$ Myr. This results in the fact that, after one crossing time, all the stars in the clusters have been affected by the radiating stars similarly, causing the scatter in the mass loss effects. While the density of each cluster defines the effects of photoevaporation in the early evolutionary stages, after one crossing time the initial density of the region is not as important and photoevaporation works uniformly.

In Figure 3.7 we show the time step of maximum mass loss for each disc. It can be seen that, other than the effect of switching on the simulation at the beginning (see section 3.4.2), there is not a particular time at which a disc loses much mass. In Figure 3.8 we show how the cumulative distributions of disc masses at different moments in the simulation. The solid lines correspond to $\rho_{100}$ the dashed lines to $\rho_{50}$. Each line corresponds to the total discs in all simulations. It can be seen that disc mass distributions decrease monotonically.

It is important to note that the FRIED grid has a lower limit of 10 $G_0$ for the FUV field, which is higher than the minimum experienced in the $\rho_{50}$ region. However, more than 90% of the stars in these simulations are within the limits of the grid at all times. In the few cases where stars were outside the limits of the grid, the mass loss obtained reflects a lower bound defined by the grid, but this does not affect our results.

Photoevaporation mass loss can have different effects over the gas and dust components
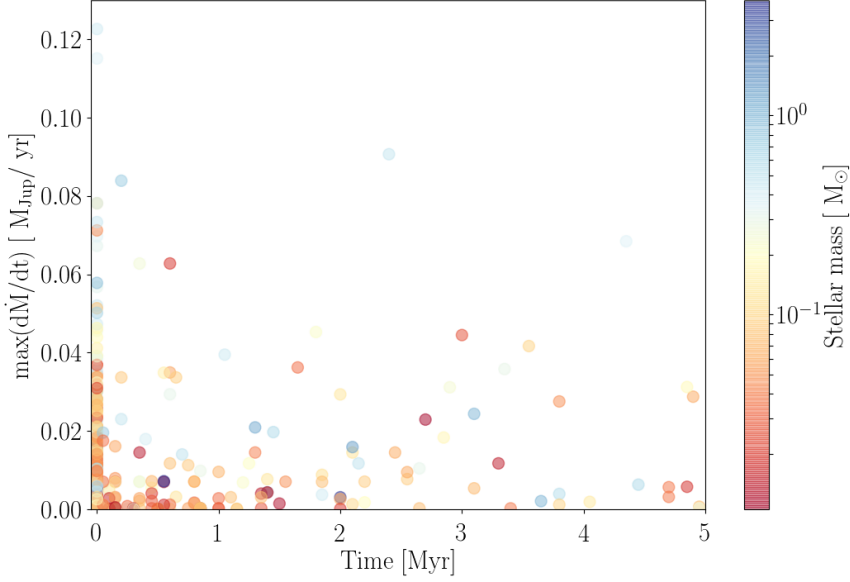
Figure 3.7: Maximum mass loss per time step for every disc. Each point corresponds to one disc in a simulation. The position of each point in time corresponds to its moment of maximum mass loss. This moment in time is not necessarily when the disc was dispersed.
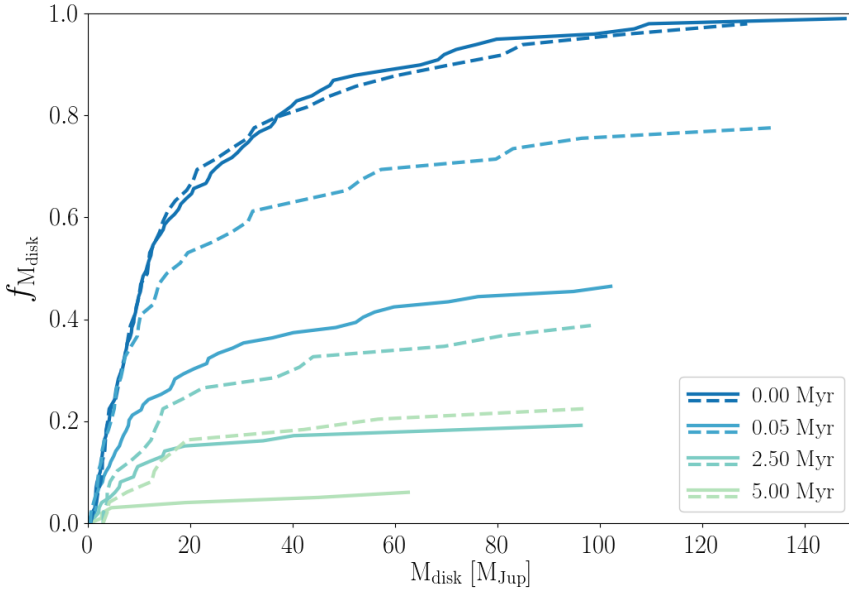


Figure 3.8: Cumulative distribution of disc masses at different simulation times. The solid lines correspond to the $\rho_{100}$ region and the dashed lines correspond to the $\rho_{50}$ region. Each curve shows the total number of discs in all simulations.

of a circumstellar disc. We expand on the consequences of this for our results in section 4.2.4.

### 3.3.2. Disc lifetimes

The lifetime of circumstellar discs in young cluster regions is an important criterion to determine how photoevaporation affects planet formation. In Figure 3.9 we show disc fractions at different times of cluster evolution (black lines), together with observed disc fractions from Ribas et al. (2014) and Richert et al. (2018). The orange line shows the mean of the observations, calculated using a moving bin spanning 10 observation points. The calculation of the mean starts by binning the first 10 points, and then sliding horizontally through the observations one point at a time such that 10 points are always considered.

The relaxation time is defined as:

$$t_{relax} = 0.138 \frac{N}{\log(\gamma N)} t_{dyn} \qquad (3.10)$$

(Spitzer 1988), where $N$ is the number of stars, $\gamma = 0.4$, and the dynamical time is:

$$t_{dyn} = \sqrt{\frac{R^3}{GM}}, \qquad (3.11)$$

where $R$ is the radius of the cluster and $M$ is its total mass. The relaxation time depends on the number of stars and the radius and mass of the stellar cluster. These are values that change through the dynamical evolution of a cluster, meaning that the relaxation time can grow and shrink at different time steps. These variations result in the jagged lines in Figure 3.9.

For the simulations shown in Figure 3.9, $t/t_{relax} = 0.5$ is reached at $t = 2.01 \pm 0.37$ Myr of evolution for $\rho_{100}$ and at $t = 2.05 \pm 0.35$ Myr for $\rho_{50}$. Disc fractions in the $\rho_{100}$ simulations drop to around 20% before 2 Myr of cluster evolution. In the regions with $\rho_{50}$ the discs survive longer, but still most of the discs have disappeared by the end of the simulations.

Planet formation could still occur in discs that have been affected by photoevaporation as long as they are not completely dispersed. For gas giant cores and rocky planets to form, protoplanetary discs need to have a reservoir of dust mass $M_{dust} \gtrsim 10M_\oplus$ (Ansdell et al. 2018). In Figure 3.10 we show the fraction of discs with solid masses $M_{disc} > 10M_\oplus$ in time, for both simulated stellar densities. We use a 1:100 dust:gas mass ratio to turn the total disc mass into dust mass. For the $\rho_{100}$ regions the number of discs that fulfil this mass requirement drops to around 20% at 1 Myr, with less than 10% of discs of said mass still present at the end of the simulations. For the less dense regions, at the end of the simulations around 20% of discs with masses $M_{disc} > 10M_\oplus$ survive.

In order to make a parallel with the Solar System, in Figure 3.11 we show the number of discs in time with radii higher than 50 au, for both density regions. The drop in disc sizes is slower than the drop in disc masses as seen in Figure 3.10, and in the $\rho_{50}$ case the fraction of discs with radius > 50 au increases in the first time steps. This is related to the fact that, while some low mass discs get destroyed, others discs are still expanding due to viscous evolution. Some of these $R_{disc} > 50$ au discs could still have masses or surface densities that are too low to form a planetary system.
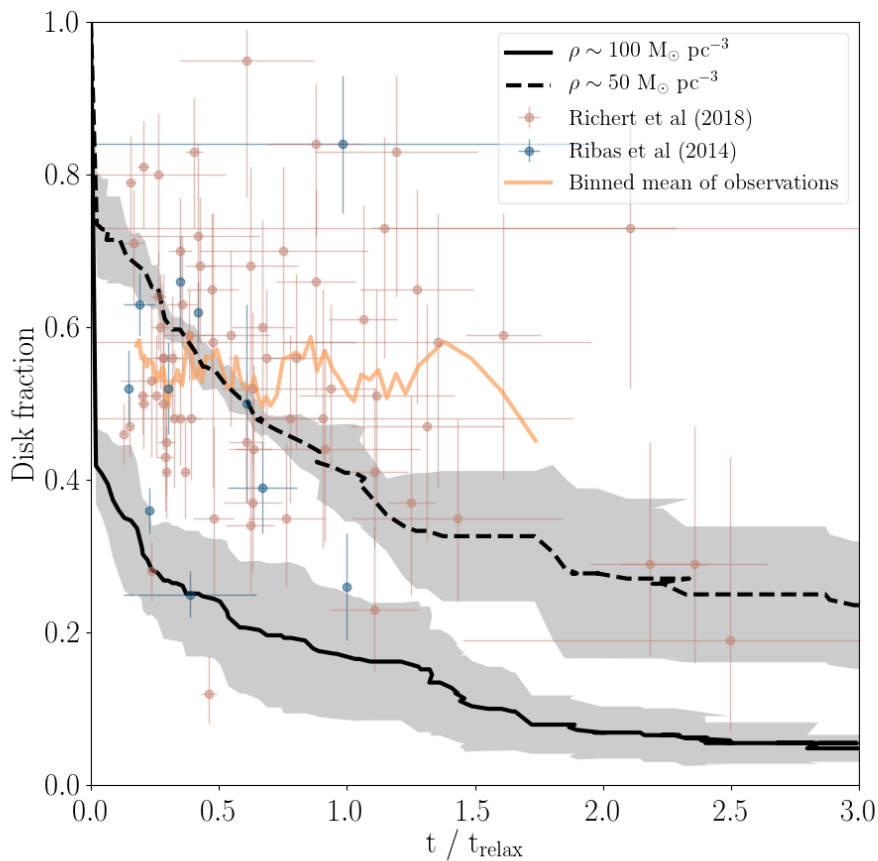
Figure 3.9: Fraction of stars with discs as a function of time. The solid black line shows the results for $\rho_{100}$ and the dashed black line for $\rho_{50}$ . The grey shaded areas indicate the standard deviation of the simulations. Observed disc fractions in star forming regions of different ages are shown for comparison. The orange line shows the mean of the observations, calculated using a moving bin spanning 10 observation points.
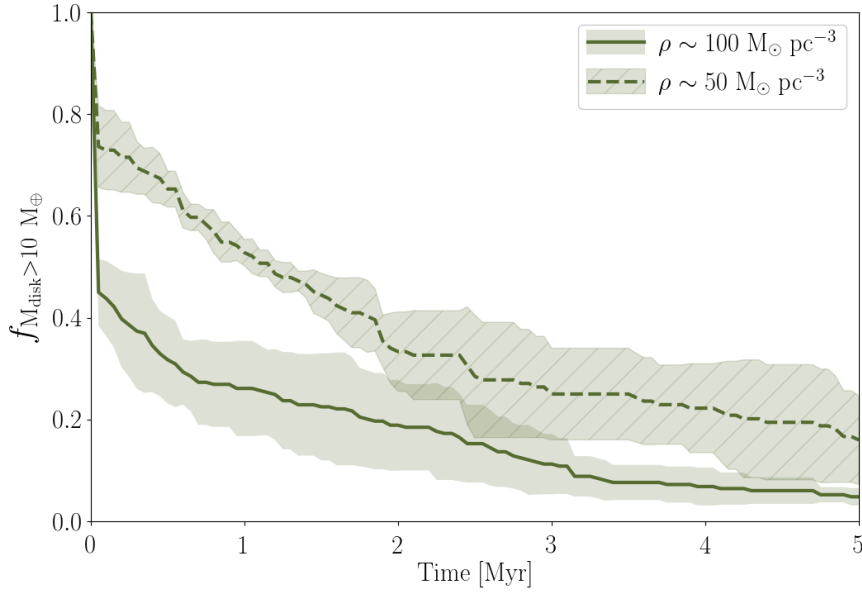
Figure 3.10: Fraction of discs with masses $M_{disc} > 10M_\oplus$ in time, for regions of different stellar densities. The shaded areas indicate the standard deviation of the simulations.



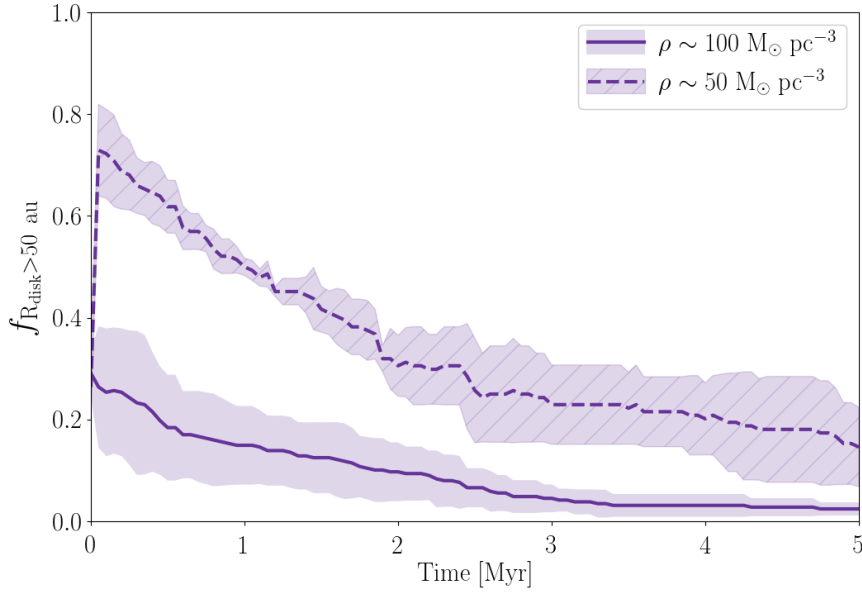Figure 3.11: Fraction of discs with radius $R_{disc} > 50au$ in time, for regions of different stellar densities. The shaded areas indicate the standard deviation of the simulations.

## 3.4.  Discussion

### 3.4.1.  Disc survival and consequences for planet formation

The results of the simulations carried out in this work characterize external photoevaporation as an important mechanism for disc dispersion. In comparison, the effect of dynamical truncations is negligible as a means for disc destruction.

The mean radiation received by the stars in our simulations fluctuates around $\sim 500\,G_0$ for the $\rho_{100}$ region and around $\sim 50\,G_0$ for the $\rho_{50}$ region. The FUV flux in the ONC is estimated to be $\sim 3 \times 10^4\,G_0$ (O'dell & Wen 1994). Kim et al. (2016) estimate $\sim 3000\,G_0$ around a B star in NGC 1977, a region close to the ONC. According to this and to our results, most of the discs in such a dense region would be destroyed before reaching 1 Myr of age. Figure 3.9 also agrees with results by Facchini et al. (2016) and Haworth et al. (2017), which show that photoevaporation mass loss can be important even for regions with $\sim 30\,G_0$ and $\sim 4\,G_0$, respectively. In particular, our results for the $\rho_{50}$ region show that even very low FUV fields can be effective in dispersing circumstellar discs over time. Winter et al. (2020b) find similar dispersion timescales, with a median of 2.3 Myr in the solar neighbourhood and 0.5 Myr in the central regions of the Milky Way, for stars down to $0.8 M_\odot$. Comparable results are obtained by Nicholson et al. (2019), who find the half life of protoplanetary discs to be around $2 - 3$ Myr in clusters of various initial conditions.

Protoplanetary discs need to have a reservoir of dust mass $M_{dust} \gtrsim 10 M_\oplus$ to be able to form the rocky cores of giant gas planets (Ansdell et al. 2018). Manara et al. (2018) show that such cores need to be already in place at ages $\sim 1 - 3$ Myr for this type of planets to form. Figure 3.10 is in agreement with these conclusions. In our simulations, by 1 Myr around 20% of the discs have masses $\gtrsim 10 M_\oplus$. This number drops to $\sim 10\%$ by 3 Myr. According to our results rocky planets and gas giant cores must form very early on, otherwise the protoplanetary discs are not massive enough to provide the necessary amount of solids. This is in agreement with observational time constrains for planet formation and with the so-called "missing-mass" problem: solids mass measurements in protoplanetary discs are lower than the observed amount of heavy elements in extrasolar planetary systems around the same type of stars (see e.g. Manara et al. 2018; Najita & Kenyon 2014; Williams 2012; Greaves & Rice 2010, for discussions on this topic). Two scenarios have been proposed to explain this discrepancy in disc and exoplanet masses. The first one suggests that planet cores emerge within the first Myr of disc evolution, or even during the embedded phase while the disc is still being formed (e.g. Williams 2012; Greaves & Rice 2010). The second scenario proposes that discs can work as conveyor belts, transporting material from the surrounding interstellar medium towards the central star (e.g. Throop & Bally 2008; Kuffmeier et al. 2017).

Disc dispersal is not homogeneous across stellar types. There are observational indications that disc dispersion timescales depend on the mass of the host star, and that less massive ($\sim 0.1 - 1.2\,M_\odot$) stars keep their discs for longer than massive stars (Carpenter et al. 2006, 2009; Luhman & Mamajek 2012). We do not see this effect in our simulations, where the most massive stars keep their discs for longer simply because they initially have the most massive discs. The same effect is observed in Winter et al. (2020b), who used an analytic approach to estimate protoplanetary disc dispersal time scales by external photoevaporation. The discrepancy between observations and theoretical results suggests that internal processes not considered in this work can also play an important role in disc dispersal. Radial drift of dust, fragmentation of large grains, and planetesimal formation are observed mechanisms that can affect both disc lifetimes and observed disc sizes. Viscous evolution alone is another internal process that can contribute to disc dispersal. A more complete model of disc evolution is needed to include the interplay between internal and external dispersion processes.

Initial disc masses are currently highly uncertain. Our chosen value of $M_d(t = 0) = 0.1M_*$ is arbitrary, but discs of higher masses could still be stably supported (Haworth et al. 2018a; Nixon et al. 2018).

Once a planetary system has formed, its survival inside a star cluster is not guaranteed. Of the 4071 exoplanets confirmed to date, only 30 have been found inside star clusters. Cai et al. (2019) performed simulations of planetary systems in dense, young massive star clusters. They found that the survival rate is $< 50\%$ for planetary systems with eccentricities $e \sim 0.05$ and semi-major axes $< 20$ au over 100 Myr of evolution. van Elteren et al. (2019) find that, in regions such as the Trapezium cluster, $\sim 30\%$ of planetary systems are affected by the influence of other stars. Their fractal initial conditions provide local regions of higher densities, which are more favourable for dynamical encounters than our initial conditions. When making parallels with currently observed exoplanet systems, it is important not only to consider the environment effects on the early protoplanetary discs, but also on the planets themselves once they are already formed.

Observations suggest that planets are able to circumvent all of these adversary processes and still form in highly unlikely regions. Evidence of star formation and even proplyd-like objects have been observed around Sgr A* (Yusef-Zadeh et al. 2015, 2017). Free-floating planets have been observed in the galactic center, and efficiency analyses of these detections suggest that there are many more yet to be observed (e.g. Ryu et al. 2020; Navarro et al. 2020).

## 3.4.2.   Influence of initial conditions

The effect of switching on photoevaporation when our simulations start have dramatic consequences for the initial circumstellar discs. Mass loss due to photoevaporation occurs very quickly once the stars are immersed in the FUV field. Around 60% and 20% of the discs are dispersed within the initial 50 000 yr in the $\rho_{100}$ and $\rho_{50}$ regions, respectively. The mean mass of the host stars whose discs dispersed in the initial 50 000 yr is $0.17 \pm 0.03M_\odot$ for the $\rho_{100}$ region and $0.14 \pm 0.04M_\odot$ for the $\rho_{50}$ region. In Figure 3.12 we show the disc fractions in time, separately for stars with masses $M_* < 0.5M_\odot$ and $M_* \geq 0.5M_\odot$. It can be seen that, for the stars of masses $M_* < 0.5M_\odot$, the disc fractions drop much more dramatically during the first thousand years of cluster evolution.

In reality, if circumstellar discs do form around such low mass stars, they could be sheltered from photoevaporation by interstellar gas and dust, which can linger for several million years after star formation (Portegies Zwart et al. 2010). Models of the Cygnus OB2 region by Winter et al. (2019a) demonstrate that the extinction of FUV photons through the gas dampens the mass loss of the discs, increasing their lifetimes. They show that Cygnus OB2 probably underwent a primordial gas expulsion process that ended $\sim 0.5$ Myr ago. This is based on the fact that 0.5 Myr of exposure to FUV fields reproduces the observed disc fractions in the region. Given that the estimated age of Cygnus OB2 is $3 - 5$ Myr (Wright et al. 2010) the primordial gas in the region insulated the discs from external photoevaporation for several Myr. A similar point is made by Clarke (2007), who propose that the FUV field of the star $\theta_1$ Orionis C must have been "switched on" no more than $1 - 2$ Myr ago to explain the disc size distribution observed around it. This switching on could have been caused by the star clearing out the primordial gas it was embedded in, thus reducing extinction around it and making its effective radiation field stronger (Ali & Harries 2019). The presence of gas in young star clusters could then protect the protoplanetary discs and make the disc fraction drop more smoothly than what is shown in Figure 3.9.

The observations shown in Figure 3.9 span clusters of many different ages and densities. Our simulation results show that one order of magnitude difference in initial cluster
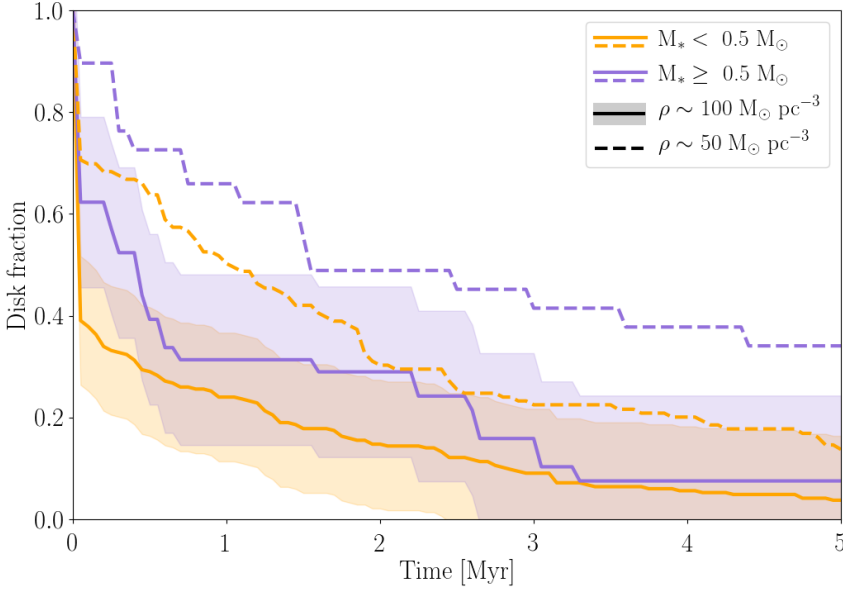
Figure 3.12: Disc lifetimes for stars $M_* < 0.5 M_\odot$ (orange) and $M_* \geq 0.5 M_\odot$ (purple). The shaded areas indicate the standard deviation of the simulations. For clarity, only the standard deviation for $\rho_{100}$ is shown, but the one for $\rho_{50}$ is of similar magnitude.

density can yield an important difference in the number of surviving discs. A one order of magnitude spread in cluster density translates to a three order of magnitude difference in cluster radius. The extent of stellar densities in regions where circumstellar discs have been detected does not only reflect the environment of these regions, but also the variety in initial cluster densities.

The initial spatial distribution of the stars in the simulations also plays an important role during the early stages of disc evolution. The stars in our simulations were initially distributed in a Plummer sphere with a specified radius and in virial equilibrium. An approach with fractal or filamentary (e.g. Winter et al. 2019a) initial conditions could change the overall disc survival rates. If a massive star is born in a clump of a fractal distribution, for example, stars in other clumps without massive stars could be minorly affected by radiation and have higher chances of surviving and, eventually, making planets. Higher density regions also increase the relevance of dynamical truncations. This effect of initial conditions could also be counteracted by dynamical mass segregation, in which massive stars move towards the center of the cluster. This would increase the effect of photevaporation in the central regions of the cluster.

### 3.4.3.    Model caveats

There are several physical processes not considered in this work which could affect the results presented here. One big caveat of our model is the lack of separation between dust and gas components in circumstellar discs. These separate disc components evolve differently and are affected in distinctive ways by outside mechanisms such as the ones implemented in this work. Gas discs has been observed to be larger than dust discs by a factor of $\sim 2$ (Ansdell

et al. 2018). Whether this is caused by different evolution for gas and dust or observational optical depth effects is still up for debate (see e.g. Birnstiel & Andrews 2013; Facchini et al. 2017; Trapman et al. 2019, for discussions on the topic). The dust in protoplanetary discs is subject to radial drifting and radially dependent grain growth, which can make it resilient to photoevaporation. This can have direct implications on the photoevaporation mass loss rates (Facchini et al. 2016; Haworth et al. 2018a) and consequences on planet formation. The conclusions regarding planet formation timescales derived in this work only consider the life expectancy of the discs, but considering different dust and gas disc components will likely affect these results.

While photoevaporation is considered to be primarily damaging for discs when coming from external sources, under certain regimes the photons coming from the host star can also contribute to disc dispersal. Gorti et al. (2009) and Gorti & Hollenbach (2009) show that FUV photons from the host star can drive photoevaporation mass loss at disc radius $\sim 1 - 10$ au and $\gtrsim 30$ au. Owen et al. (2010) and Font et al. (2004) show that internal photoevaporation can also remove loosely bound material from the outer regions, however the largest mass loss was from the inner $\sim 20$ au region. Fatuzzo & Adams (2008) and Hollenbach et al. (2000) find that external photoevaporation dominates for disc regions $> 10$ au. The approach used in this work is valid for the disc truncation approximation, however, a more complete analysis would have to consider the combined action and interplay of external and internal photoevaporation.

Mass loss due to photoevaporation was modelled by calculating a truncation radius and removing all the mass outside it, while the inner region of the disc remained unperturbed. In reality, external FUV radiation can heat the whole surface of the disc, and mass loss can occur not just as a radial flow but also as a vertical flow from all over the disc (Adams et al. 2004). Given that the mass in the outer regions of a disc is more loosely bound to its host star, the truncation approach is a good first order approximation for mass loss. Furthermore, the FRIED grid used to estimate the photoevaporation mass loss was built using a 1-dimensional disc model. New simulations by Haworth & Clarke (2019) show that, when considering a 2-dimensional disc model, mass loss rates can increase up to a factor 3.7 for a solar mass star. The photoevaporation mass losses obtained in this work should then be considered as lower limits, but are still a good estimate of the effects of bright stars in the vicinity of circumstellar discs.

In the present work we did not include binary stars or any multiples. The presence of multiple stellar systems can have direct consequences on the dynamical evolution of the cluster and on the effects of photoevaporation over the discs. Discs around binary stars have been observed in the star forming regions $\rho$ Ophiuchus (Cox et al. 2017) and Taurus-Auriga (Harris et al. 2012; Akeson & Jensen 2014; Akeson et al. 2019). Observations suggest that these discs are more compact and less bright than the ones around isolated stars. Discs around binary stars might also have shorter lifetimes, due to effects of the companion on the viscous timescale of the disc and also because of photoevaporation inside the system (Shadmehri et al. 2018; Rosotti & Clarke 2018).

Another process that can have important consequences in the evolution of circumstellar discs are supernovae explosions. Close & Pittard (2017) showed that nearby (0.3 pc) supernova explosions can cause mass loss rates of up to $1 \times 10^{-5} \, M_\odot \mathrm{yr}^{-1}$ which can be sustained for about 200 yr. Only discs that are faced with the flow face-on manage to survive, but still lose 50% of their mass in the process. Portegies Zwart et al. (2018) show that a supernova explosion at a distance between 0.15 and 0.4 pc could create a misalignment of $\sim 5°.6$ between the star and its disc, which is consistent with the inclination of the plane of the Solar System. Such an event would also truncate a disc at around the edge of the Kuiper belt

$(42 - 55\,\mathrm{au})$. Similar effects can be caused by other outcomes of stellar evolution, such as winds (Pelupessy & Portegies Zwart 2012).

## 3.5. Conclusions

We perform simulations of star clusters with stellar densities $\rho \sim 100\,\mathrm{M_\odot\,pc^{-3}}$ and $\rho \sim 50\,\mathrm{M_\odot\,pc^{-3}}$. The stars with masses $\mathrm{M_*} \leq 1.9\,\mathrm{M_\odot}$ are surrounded by circumstellar discs. Stars with masses $\mathrm{M_*} > 1.9\,\mathrm{M_\odot}$ are considered sufficiently massive stars to emit UV radiation, causing the discs around nearby stars to evaporate. The discs are subject to viscous growth, dynamical encounters, and external photoevaporation. The simulations span $5\,\mathrm{Myr}$ of cluster evolution. The main results of this work are:

1. In clusters with density $\rho \sim 100\,\mathrm{M_\odot\,pc^{-3}}$ around 80% of discs are destroyed by external photoevaporation within $2\,\mathrm{Myr}$. The mean background FUV field is $\sim 500\,\mathrm{G_0}$.

2. In clusters with density $\rho \sim 50\,\mathrm{M_\odot\,pc^{-3}}$ around 50% of discs are destroyed by external photoevaporation within $2\,\mathrm{Myr}$. The mean background FUV field is $\sim 50\,\mathrm{G_0}$. This shows that even very low FUV fields can be effective at destroying discs over long periods of time.

3. Mass loss caused by dynamical encounters is negligible compared to mass loss caused by external photoevaporation. Disc truncations that result from dynamical encounters are not an important process in setting observed disc size and mass distributions.

4. At $1\,\mathrm{Myr}$, $\sim 20\%$ of discs in the $\rho \sim 100\,\mathrm{M_\odot\,pc^{-3}}$ region and $\sim 50\%$ of discs $\rho \sim 50\,\mathrm{M_\odot\,pc^{-3}}$ region have masses $\mathrm{M_{disc}} \geq 10\,\mathrm{M_\oplus}$, the theoretical limit for gas giant core formation.

5. Our results support previous estimations that planet formation must start in timescales $< 0.1 - 1\,\mathrm{Myr}$ (e.g. Najita & Kenyon 2014; Manara et al. 2018).

6. The obtained disc fractions in the different density regions, together with the quick dispersion of the discs in all the simulations, suggest that initial conditions are very important in the development of models of early protoplanetary disc evolution.

## Acknowledgements

## 3.A. Resolution of the discs

We use a resolution of 50 cells for the discs which gives us a good trade-off between computing time and acceptable results. In isolated disc evolution this causes an overestimation of disc radius by $\sim 10\%$ on average over 1 Myr of disc evolution, compared with higher

resolutions (Figure 3.13). Since all the discs in the simulation are affected by photoevaporation from the start, no discs evolve as in the isolated case. Disc masses are overestimated by less than ∼ 5% compared to higher resolution runs (Figure 3.14). This results, in turn, in a slight underestimation of the effects that mass removal, whether through photoevaporation or dynamical encounters, has on the survival times of the discs. Given that we define a disc as dispersed when it has lost ∼ 90% of its initial mass, the slight mass overestimate obtained with the 50 cells resolution does not reflect in a quicker evaporation of the discs.
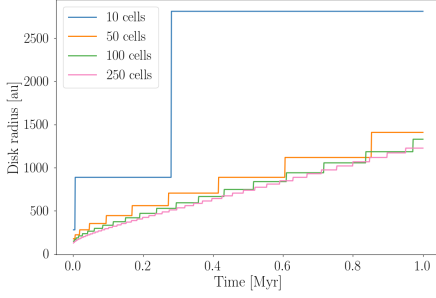


Figure 3.13: Disc radius in time for different resolutions, for a disc evolving in isolation for 1 Myr.
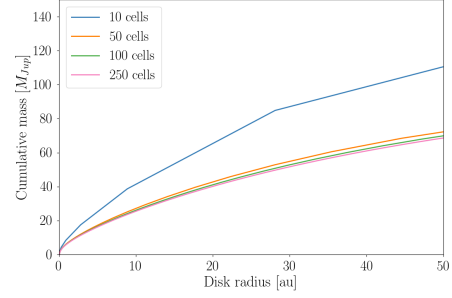


Figure 3.14: Cumulative disc mass for different resolutions, for a disc evolving in isolation for 1 Myr.

❋ ❋ ❋